JOURNAL LA MULTIAPP

VOL. 05, ISSUE 02 (044-051), 2024
DOI: 10.37899/journallamultiapp.v5i2.1006

Algorithm for Detecting Acoustic Traces of Neutrino Decay

Askold Belyakov[1]

[1]*Institute Physics of Earth Russian Academy of Sciences, Moscow, Russia*

**Corresponding Author: Askold Belyakov*
Email: askbel32@gmail.com

Article Info

Article history:
Received 17 August 2021
Received in revised form 06 September 2021
Accepted 19 September 2021

Keywords:
Detection algorithm
acoustic traces of neutrino decay
ultra-sensitive magnetoelastic geophone
electromagnetic field sensor
Nyquist frequency
Earth
Space

Abstract

*In the articles "Doppler Effect and Acoustic Trails of Neutrinos" and "Neutrinos above the Earth's surface", published in the journal "LA MULTIAPP" on February 25, 2022 and July 12, 2023, I was forced to touch on the astrophysical topic when, in the flow of data obtained in the process Monitoring acoustic noise with a recorder with a Nyquist frequency of 5 kHz, at a depth of 1000 m in the earth's crust, events began to be frequently observed, the shapes and frequencies of which are not typical for seismology and geophysics, and had not previously been observed by anyone. The shape of some events was very similar to the traces of neutrino decay, such as the bipolar pulse and the "diamond", recorded by acoustic detectors in seawater. Subsequently, when recording high-frequency acoustic processes on the Earth's surface with a recorder with a Nyquist frequency of 50 kHz, events were discovered that were even more similar to traces of neutrino decay. At the same time, a **"strange"** association of some events of unknown origin with the field extrema of the power electrical network of a large city was discovered. To avoid erroneous conclusions, it is necessary to understand the origin of this **"strangeness"**.*

Introduction

After extensive testing at the University of Texas at Austin from June 2021 to June 2023, the MIG-3V geophone was returned, which made it possible to continue observations and occasionally record fragments of the acoustic noise of a large city with an ultra-sensitive geophone (Wang et al., 2022; Grineski et al., 2023). Additionally, a separate coil of the vertical channel of the MIG-3V geophone was used as an electromagnetic field sensor at the recording site. This was necessary to explain the "strange" association of some events with extrema of electromagnetic field amplitudes (Smith et al., 2023; Kahn et al., 2022). There is little confidence that several short (10-15 sec.) recording sessions will record the same successful moments as February 25, 2023, but not trying to explain the detected "oddities" would be an unforgivable mistake. As a result, this turned out to be possible, and high-frequency pulsed events were sometimes detected in short recording sessions.

Methods

Below, in Fig. 1, shows the installation of the MIG-3V geophone (2), attached to the inner surface of the wall on the second floor of a wooden house, and a separate coil of the vertical channel of the MIG-3V geophone (3), as a sensor of the vertical component of the electromagnetic field with a frequency of 60 Hz and a sensor of the geophone MIG -3V without housing (1), used previously. The recording system consists of ZET 410 preamplifiers with possible gains of 1, 10, 100, 1000 and a ZET 230 ADC module with four 24-bit ADCs, the maximum sampling frequency of which is 100 kHz, controlled by a computer. The module operates in the mode of inputting digital signals to the hard drive of a personal computer or external drive in the form of *.ana-*.anp files. ZETLab software allows you to begin the

ISSN: 2716-3865 (Print), 2721-1290 (Online)

registration process immediately after launching the program. For two horizontal registration channels: X - directed perpendicular to the southern wall of the house and Y - directed parallel to the wall, the gain factors are set to 1000, and for Z - the vertical channel and E - the electromagnetic field sensor - 10. This decision is explained by the high level of electromagnetic interference in the area observations that go beyond the recording range of the vertical channels Z and E, while the horizontal channels of the geophone, which have internal protection from electromagnetic fields, allow the use of maximum gain.

Figure 1. – MIG-3V geophone sensor, 2 – MIG-3V geophone,

Coil of The Vertical Channel of The MIG-3V Geophone

It is assumed that before analysis, all data will be adjusted taking into account the amplifier coefficients and the sensitivity of the geophone channels to be able to correctly determine the vector direction to the intended signal source. The resulting *.ana-*.anp files are entered into the WinABD program database, which allows visualization of time series, their various transformations and evaluations. In particular, in relation to the series under consideration, the following is carried out compensation for the shift of the average value, increasing the amplitudes of vertical channels so that all four channels have equal sensitivity, calculating the absolute rate of change in the signal amplitude and spectral analysis of selected channels and fragments. The totality of the results obtained is analyzed using the WinABD program and conclusions are drawn about the presence of acoustic traces of neutrino decay. Additionally, at the preliminary stage, registered files can be converted into *.wav files for listening by professional geoacoustic or hydroacoustics. As a result, one of the algorithms for detecting high-frequency signals against a background of low-frequency noise may look like this: 1. Three components of the vector of the original signal from the geophone, through high-quality analog amplifiers, are brought to the same sensitivity, taking into account the real sensitivity of the horizontal and vertical channels, and are fed to the audio system for listening; 2. The same three components of the original signal are fed to the inputs of analog amplifiers of the recording system, the sensitivity of which is set so that the signals do not go beyond the measurement limits. The recording system program is configured to continuously record files of the required length at a sampling rate of 100 kHz; 3. The resulting *.ana-*.anp files are saved on external media and simultaneously transferred to the WinABD program, which converts them into time series; 4. The constant offset is removed from the time series and the amplitude is adjusted taking into account the sensitivity of each of the geophone channels and the set gain of the pre-amplifier, which allows, using normalized series of three orthogonal directions, to determine the direction to the signal source relative to the observation location at each point in time; 5. The normalized series are converted into series of the absolute rate of change in signal amplitudes, which increases the possibility of detecting high-frequency events even against the background of prevailing low-frequency interference.

ISSN: 2716-3865 (Print), 2721-1290 (Online)

K = K1 · K2 · K3 where:

K1 - sensor electromechanical coupling coefficient – 0.6 (0.15) $mV \cdot s^3 \cdot m^{-1}$;

K2 - preamplifier coefficient: 1, 10, 100. 1000 – 10^3;

K3 - transfer coefficient of the analog-to-digital converter - 1.

$K = 0.6 \cdot 10^3 \cdot 1\ mV \cdot s^3 \cdot m^{-1}$

The measured parameter (acceleration rate) - R [$m \cdot s^{-3}$] is determined by the formula R = N / K, where N is the number of "mV" at the output of the ADC.

For example, at N = 1 mV, $R1 = 1 / 0.6 \cdot 10^3\ mV \cdot s^3 \cdot m^{-1} = 1.66\ m \cdot s^{-3}$.

To determine the amplitudes of acceleration - a, speed - v or displacement - L at

N = 388 (double amplitude, peak-to-peak, mV), it is necessary to divide the calculated parameter R = 644 by 2πf to the first, second and third powers, respectively.

1. f, Hz	2. 2πf	3. $(2\pi f)^2$	4. $(2\pi f)^3$
5. 50000	6. $314 \cdot 10^3$	7. $98 \cdot 10^9$	8. $31 \cdot 10^{15}$

Factors for determining R, a, v and L: (multiply N in the corresponding frequency band)

N=388 mV, f=50 kHz.

9. f, Hz	10. R, $m \cdot s^{-3}$	11. a, $mm \cdot s^{-2}$	12. v, $nm \cdot s^{-1}$	13. L, fm
14. 50000	15. 644	16. $2 \cdot 10^{-3}$	17. $6.6 \cdot 10^{-9}$	18. $21 \cdot 10^{-15}$

Results and Discussion

According to Lanza et al. (2022) The main questions to which it was necessary to find answers: Why are some high frequency pulses clearly concentrated (or synchronized) near the extreme points of the “sine wave” of the electrical network? Is this not a coincidence? Is it possible to artificially generate observable pulses in the power grid itself, as a means of monitoring or managing networks along network wires? Returning to the observations on February 25, 2023, a fragment of the data is shown in Fig. 2, it is clearly seen that the repetition frequency of groups of bipolar pulses (from one to ten) is close to the frequency of the city power grid of 60 Hz.

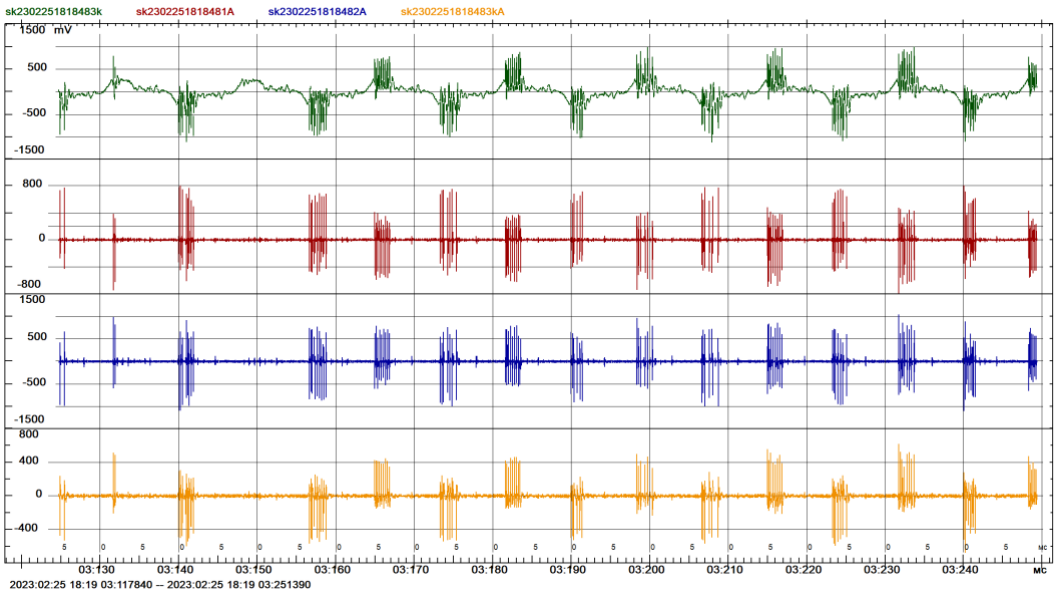

Figure 2. Fragment (134 ms) of registration on February 25, 2023

This is especially clearly visible in the upper track of the fragment of the graph of the vertical Z channel sk2302251818483, which, unlike horizontal channels, does not have differential protection from

ISSN: 2716-3865 (Print), 2721-1290 (Online)

electromagnetic fields, and the frequency of 60 Hz is noticeably observed, and the amplitude of the pulse signals is much higher than the amplitude of the interference of 60 Hz (Lu & Chen, 2022; Morris, 2020; Davis & Jorgensen, 2022). The three lower tracks X. Y and Z show fragments of graphs of the absolute rate of change in signal amplitudes, in which the amplitudes of high-frequency signals are increased and low frequency signals are decreased.

Before analyzing the processes in Fig. 2, the level of the system's own noise and its frequency composition were checked. The results for gain factors of 10 for four recording channels are shown in Figures 3 and 4. In the graphs of Figure 3 it can be seen that with preliminary amplification of 10, the amplitude of self-noise in all channels does not exceed 0.2 - 0.3 mV and does not have significant high-frequency.

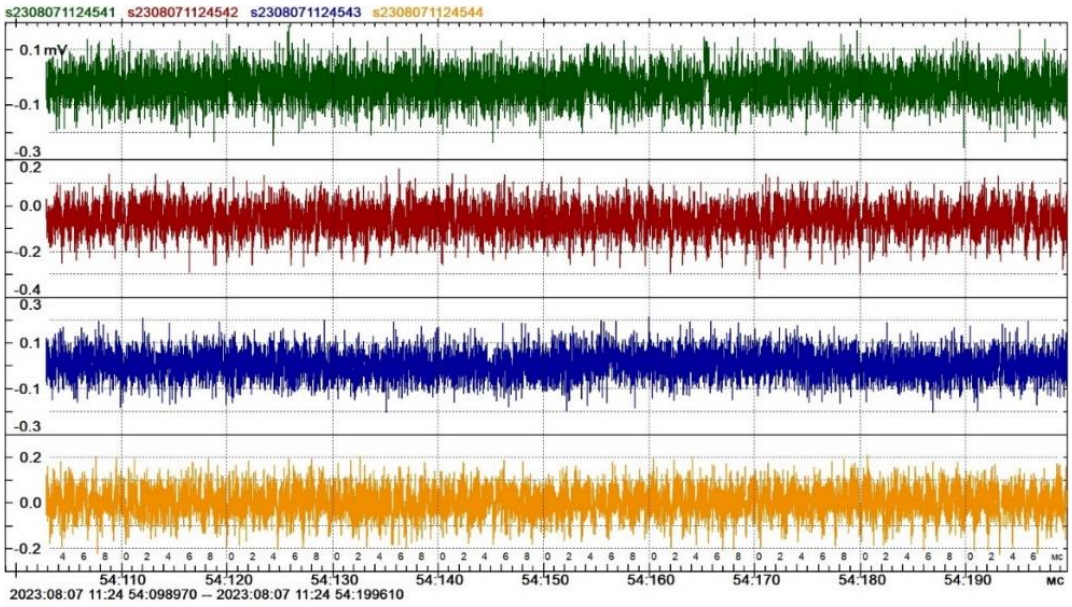

Figure 3. Internal noise of the recording system. Fragment 100 ms

Figure 4 shows that the period grams of all four channels are quite flat, uniform and without noticeable excesses in the high-frequency part. This allows us to conclude that the recording system itself does not generate high-frequency interference with frequencies approaching 50 kHz (Nyquist frequency).

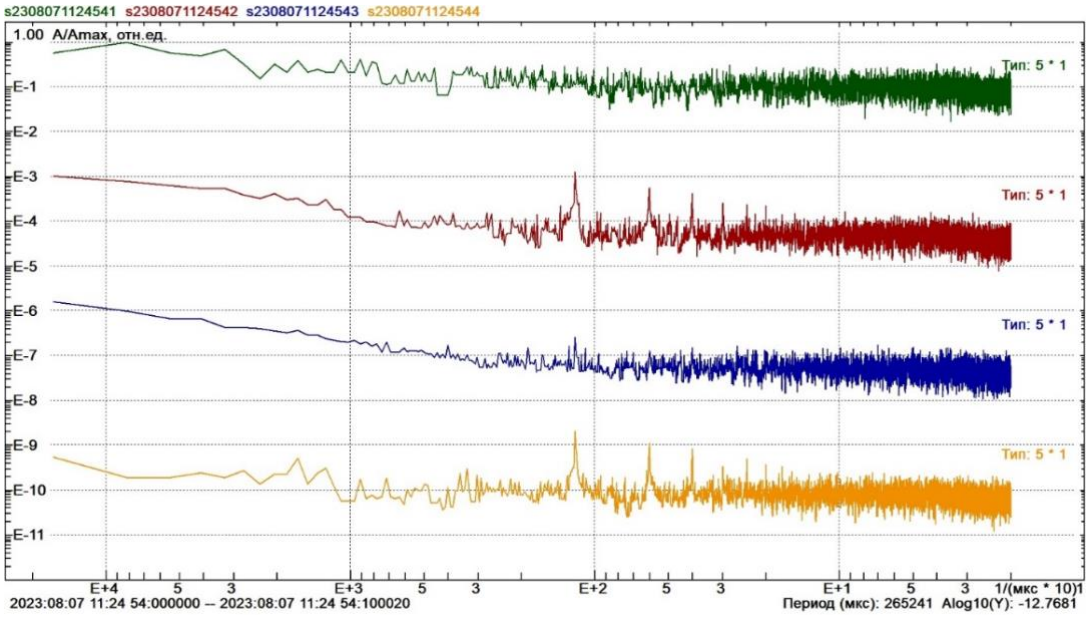

Figure 4. Period gram of the recording system's own noise

ISSN: 2716-3865 (Print), 2721-1290 (Online)

Below, in Figure 5 shows a fragment with nine unknown pulses timed to the extreme of network interference, and in Figure 6 is its period gram, which shows that the amplitudes of frequencies approaching 50 kHz fall sharply in all measuring channels.

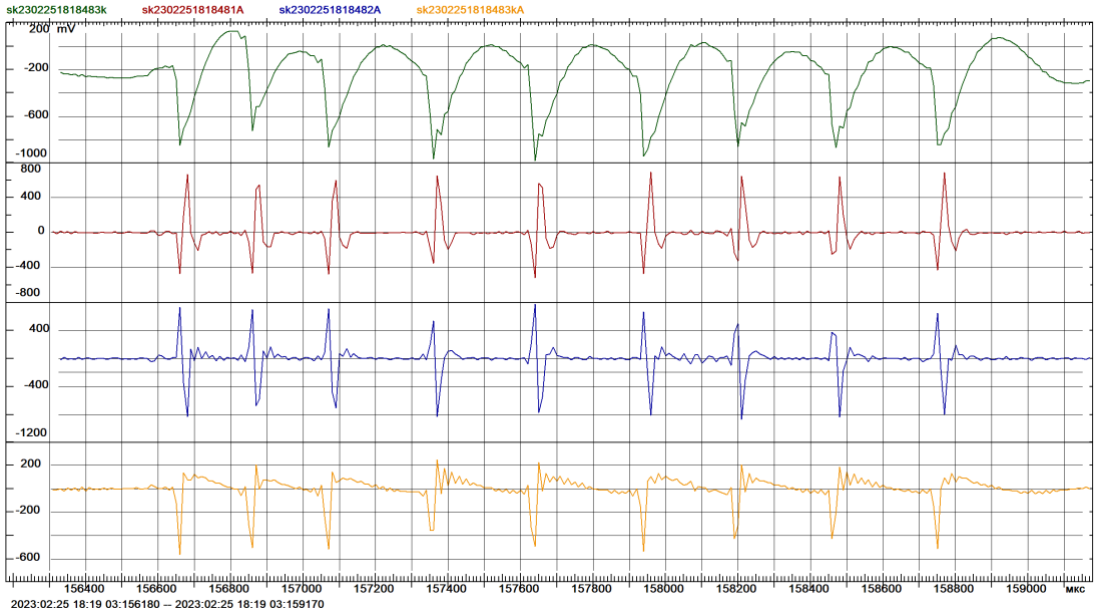

Figure 5. ms recording fragment

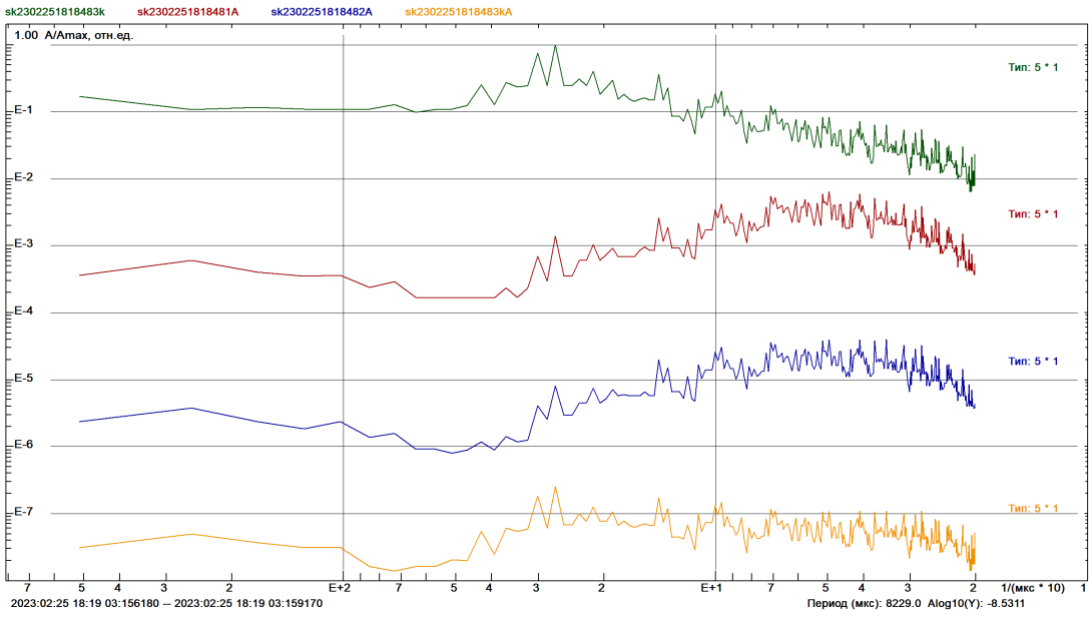

Figure 6. Periodogram of a 4 ms recording fragment

In Figure 7 shows the previous recording fragment, in which there are no large amplitude pulses, but a background is visible on which “diamond” type events are present.

ISSN: 2716-3865 (Print), 2721-1290 (Online)

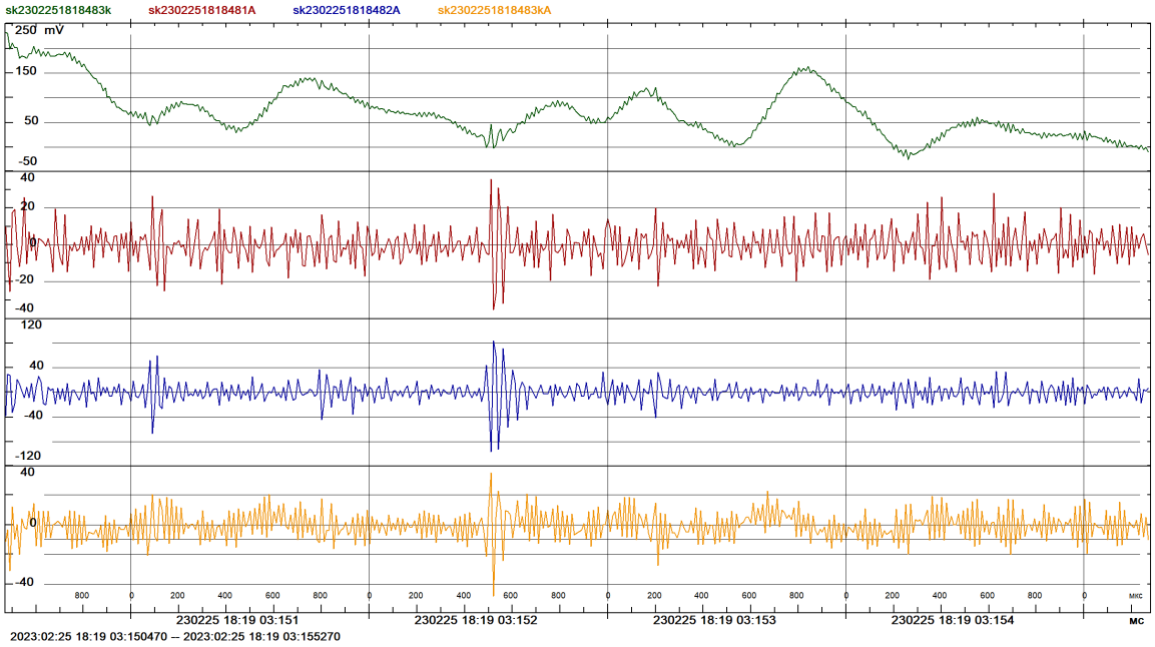

Figure 7. Fragment of registration 4.8 ms

Experts believe that diamond-type events, which are recorded by acoustic neutrino detectors in an aquatic environment, are associated with neutrino decay. This is confirmed by the period gram in Fig. 8, which shows the clear presence of a frequency of 46.3 kHz (period 21.6 μs).

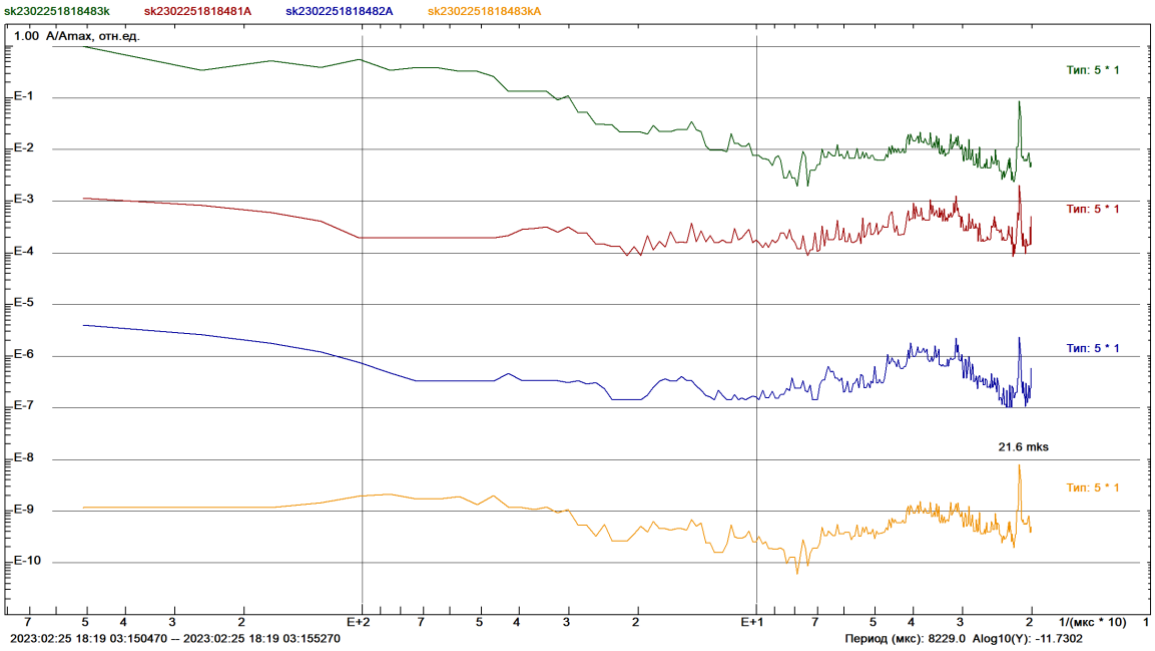

Figure 8. Periodogram of the 4.8 ms recording fragment

In Figure 9 shows a fragment of registration on December 7, 2023, in which the tested MIG-3V geophone (2) and an electromagnetic field sensor (3) are already used, and not the open geophone sensor (1), the sensitivity of which is unknown without a housing (see Fig. 1).

ISSN: 2716-3865 (Print), 2721-1290 (Online)

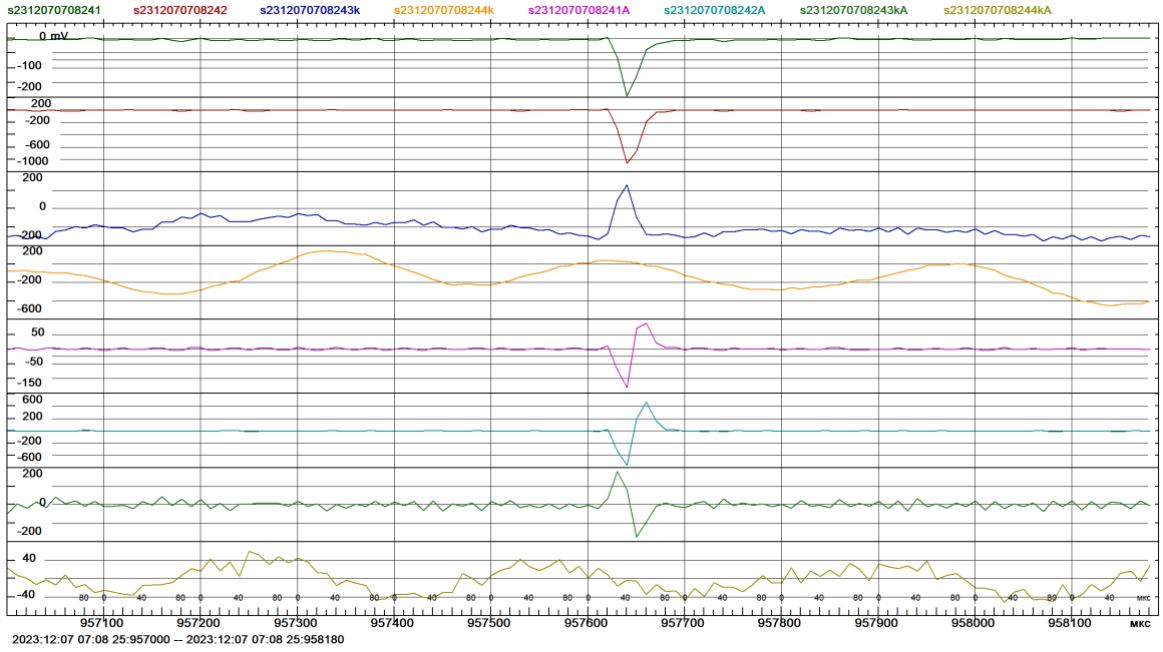

Figure 9. Fragment of registration 1.2 ms. December 7, 2023

This version of the registration system allows you to continuously calculate the direction of propagation of received signals, which provides an additional argument for their identification (Al Bassam et al., 2021; Bamakan et al., 2022). However, this is in the future, and now in Figure 9 (the three upper tracks, channels X, Y, Z) we clearly see the components of a pulse signal with a duration of 50 μs (visible frequency 20 kHz) of a fairly large amplitude. However, there is no change on the fourth track E. The same thing happens on the four lower tracks, where the rate of change in signal amplitudes is shown (Xu & Zhang, 2021). This is convincing evidence of the acoustic origin of the detected pulses, but not their connection with neutrinos, although it is difficult to propose another source of such signals.

Conclusion

The topic under consideration is very interesting and promising in the case of independent confirmation of the connection between the detected acoustic traces of neutrino decay using a relatively simple mobile instrument, Carrying out research for this purpose is currently quite simple, It is necessary to begin monitoring in a place remote from possible sources of electromagnetic fields with a frequency of 60 Hz, for example, in Yellowstone National Park, where the necessary infrastructure is available. A set of tested unique equipment for monitoring acoustic signals in solid media is available and can be rented or leased. Additionally, you will need a professional laptop with an external drive of at least 2 TB and autonomous power supply.

Acknowledgment

I am sincerely grateful to Alexey Deshcherevsky for his excellent WinABD program and his creative efforts to improve and update it. Without the WinABD program, this and many of my other works that require calculations, transformations and graphics would not exist.

References

Al Bassam, N., Hussain, S. A., Al Qaraghuli, A., Khan, J., Sumesh, E. P., & Lavanya, V. (2021). IoT based wearable device to monitor the signs of quarantined remote patients of COVID-19. *Informatics in medicine unlocked*, *24*, 100588. https://doi.org/10.1016/j.imu.2021.100588

ISSN: 2716-3865 (Print), 2721-1290 (Online)

Bamakan, S. M. H., Nezhadsistani, N., Bodaghi, O., & Qu, Q. (2022). Patents and intellectual property assets as non-fungible tokens; key technologies and challenges. *Scientific Reports*, *12*(1), 2178.

Davis, M. W., & Jorgensen, E. M. (2022). ApE, a plasmid editor: a freely available DNA manipulation and visualization program. *Frontiers in Bioinformatics*, *2*, 818619. https://doi.org/10.3389/fbinf.2022.818619

Grineski, S. E., Collins, T. W., Chakraborty, J., Goodwin, E., Aun, J., & Ramos, K. D. (2023). Social disparities in the duration of power and piped water outages in Texas after Winter Storm Uri. *American Journal of Public Health*, *113*(1), 30-34. https://doi.org/10.2105/AJPH.2022.307110

Kahn, F., Bonander, C., Moghaddassi, M., Rasmussen, M., Malmqvist, U., Inghammar, M., & Björk, J. (2022). Risk of severe COVID-19 from the Delta and Omicron variants in relation to vaccination status, sex, age and comorbidities surveillance results from southern Sweden, July 2021 to January 2022. *Eurosurveillance*, *27*(9), 2200121.

Lanza, M., Sebastian, A., Lu, W. D., Le Gallo, M., Chang, M. F., Akinwande, D., ... & Roldan, J. B. (2022). Memristive technologies for data storage, computation, encryption, and radio-frequency communication. *Science*, *376*(6597), eabj9979.

Lu, T., & Chen, Q. (2022). Independent gradient model based on Hirshfeld partition: A new method for visual study of interactions in chemical systems. *Journal of Computational Chemistry*, *43*(8), 539-555. https://doi.org/10.1002/jcc.26812

Morris, A. G. (2020). Biological relationships between Upper Pleistocene and Holocene populations in southern Africa. In *Continuity or Replacement* (pp. 131-143). CRC Press.

19. Place Lake St. sensor type MIG-3V, K1- 0.6 (0.15) $mV \cdot s^3 \cdot m^{-1}$, K2 - 10^3, K3 – 1.

Smith, D. J., Gold, J. A., Chiller, T., Bustamante, N. D., Marinissen, M. J., Rodriquez, G. G., ... & Ostrosky-Zeichner, L. (2023). Update on outbreak of fungal meningitis among US residents who received epidural anesthesia at two clinics in Matamoros, Mexico. *Clinical Infectious Diseases*, ciad570. https://doi.org/10.1093/cid/ciad570

Wang, X., Du, Z., James, E., Fox, S. J., Lachmann, M., Meyers, L. A., & Bhavnani, D. (2022). The effectiveness of COVID-19 testing and contact tracing in a US city. *Proceedings of the National Academy of Sciences*, *119*(34), e2200652119. https://doi.org/10.1073/pnas.2200652119

Xu, W., & Zhang, F. (2021). Fast-lio: A fast, robust lidar-inertial odometry package by tightly-coupled iterated kalman filter. *IEEE Robotics and Automation Letters*, *6*(2), 3317-3324. https://doi.org/10.1109/LRA.2021.3064227

ISSN: 2716-3865 (Print), 2721-1290 (Online)